Super-resolution tracking of mitochondrial dynamics with a third-row transition metal complex dye

Qixin Chen[1,2,4,*], Chengzhi Jin[3,*], Xintian Shao[1,2,4,*], Ruilin Guan[3,*], Zhiqi Tian[1], Chenran Wang[1], Fei Liu[2,4], Peixue Ling[2,4], Jun-Lin Guan[1], Liangnian Ji[3], Fengshan Wang[2], Hui Chao[3], Jiajie Diao[1]

1. Department of Cancer Biology, University of Cincinnati College of Medicine, Cincinnati, OH 45267, USA.

2. School of Pharmaceutical Sciences, Shandong University, Jinan 250101, China.

3. MOE Key Laboratory of Bioinorganic and Synthetic Chemistry, School of Chemistry, Sun Yat-Sen University, Guangzhou 510275, China

4. Shandong Academy of Pharmaceutical Science, Key Laboratory of Biopharmaceuticals, Engineering Laboratory of Polysaccharide Drugs, National–Local Joint Engineering Laboratory of Polysaccharide Drugs, Jinan 250101, China.

*These authors contributed equally to this work.

Correspondence and requests for materials should be addressed to F.W. (email: fswang@sdu.edu.cn), H.C. (email: ceschh@mail.sysu.edu.cn), or J.D. (email: jiajie.diao@uc.edu).

Abstract Combining luminescent transition metal complex (LTMC) dye with super-resolution microscopy is an excellent strategy for the long-term visualization of the dynamics of subcellular structures in living cells. However, it remains unclear whether the third-row LTMC dye is applicable for

a particular type of super-resolution technique, structured illumination microscopy (SIM), to image subcellular structures. As described herein, we developed a synthetic 970-Da third-row LTMC, Iridium(III) complex dye, to track mitochondrial dynamics in living cells under SIM. The dye demonstrated excellent specificity and photostability and satisfactory cell permeability. While using SIM to image mitochondria, we achieved an approximately 80-nm resolution that allowed the clear observation of the structure of mitochondrial cristae. We used the dye to monitor mitochondrial dynamics relative to lysosomes, including fusion involved in mitophagy, and newly discovered mitochondria-lysosome contact (MLC) under different conditions. MLC remained intact and fusion vanished when five receptors, p62, NDP52, OPTN, NBR1, and TAX1BP1, were knocked out, suggesting that these two processes are independence.

Introduction

Highly mobile and dynamic in living cells, mitochondria are the energy-generating organelles of cells[1, 2, 3], the disorder of which is associated with various diseases, including Alzheimer's, Parkinson's, and cancer[4, 5]. Recently developed super-resolution fluorescence microscopies such as stimulated emission deletion (STED)[6, 7, 8], structured illumination microscopy (SIM)[9, 10, 11], and stochastic optical reconstruction microscopy (STORM)[12, 13, 14], as well as other single-molecule super-resolution imaging techniques[15, 16, 17], have enhanced new tools for investigating the dynamics of subcellular structures, including mitochondria. At the same time, they have also added to the requirements of fluorescent dyes, which need especially low cytotoxicity and high photostability to make imaging living cells possible. Currently, imaging subcellular structures relies upon fluorescent proteins[18, 19], organic dyes[20], and quantum dots[21]; however, none of those dyes are suitable for tracking the dynamics of subcellular structures due to their poor photostability and vulnerability to photobleaching[22]. Studies have shown that using luminescent transition metal complexes (LTMCs)[23, 24, 25, 26], including Ru, Re, Pt, Au, and Zn, is an excellent alternative strategy that can overcome those drawbacks. For example, to image mitochondria, Tang et al. reported a first-row Zn complex dye whose fluorescence intensity decayed to 10% after a short period of continuous scan under STORM[27]. More recently, the lab of Jim A. Thomas developed a second-row Ru (II) complex dye with extreme photostable, long-term, large Stokes shift and subcellular targeting to image nuclear chromatin and mitochondria at a resolution of less than 50 nm under STED[28]. However, it remains unclear whether third-row LTMC dyes are applicable with SIM to image the dynamics of subcellular structures.

Among LTMC dyes, Iridium(III) complexes are the most attractive candidate for bioimaging applications due to their high phosphorescent quantum yield at room temperature, high penetration and emission spectrum that can be extended to near-infrared areas, excellent photochemical and physicochemical stability that allows for long-term imaging, high biological safety, and low cytotoxicity[4, 29]. Those unique structures and photophysical properties make it possible to develop innovative bioimaging applications based on phosphorescence.

As described herein, we developed a small molecule dye based on Iridium(III) complex for tracking mitochondrial dynamics under a SIM for the first time. The dye not only has exceptional cell permeability, light stability and mitochondrial specificity but can also allow the observation of mitochondria at up to 80-nm resolution in living cells under SIM. Moreover, the dye permits the clear observation of the structure of mitochondrial cristae, as well as the recording of dynamic approach and separation processes of mitochondria. We applied the dye to monitor fusion involved in mitophagy and mitochondria–lysosome contact (MLC) in living cells and found that five receptors, p62, NDP52, OPTN, NBR1, and TAX1BP1, for mitophagy played no role in regulating MLC upon stimulation. Our findings thus illustrate a novel perspective for using third-row LTMC dyes such as Iridium(III) complexes to image the dynamic processes of subcellular structures in living cells under SIM.

Results

Synthesis and optical characterization

First, we designed and synthesized an Iridium(III) complex dye with a molecular weight of 970 Da to

specifically image mitochondria in living cells under SIM (Fig. 1a). The main synthesis reaction route consisted of three major steps (Fig. 1b), and the characterizations with electrospray mass spectrometry and nuclear magnetic resonance spectroscopy appear in Supplementary Fig. 1-3. The dye had higher phosphorescence at a wavelength of approximately 700 nm and different optical phosphorescence characteristics in phosphate-buffered saline at pH 4-10 (Fig. 1c-d), which indicates that it can be used in living cells in different pH environments. The emission spectra show that the luminescent intensity in the range of 4-6 is relatively low compared to that in the range of 6-10. This phenomenon may contribute to the presence of pyrazine ring in the auxiliary ligands of Iridium(III) complexes. However, it is also acceptable for mitochondrial imaging (physiological pH: 6.50 to 8.20)[30], because the phosphorescence intensity of this Iridium(III) complexes is relatively stable in the range of 6.0 - 10.0. To further investigate the optical properties of the dye in other solvent media, we performed fluorescence detection in 100% fetal calf serum (FBS) and Dulbecco's modified eagle medium (DMEM; Supplementary Fig. 4a-b). The dye exhibited high fluorescence intensity in FBS and low fluorescence in DMEM, which indicates that it can obtain a lower background in DMEM under SIM. Upon testing the phosphorescence properties of the dye at different temperatures, we found that it had the same optical properties at all temperatures tested (Supplementary Fig. 4 c-d), which suggests using the dye can afford consistent data acquisition at physiological temperature (37 ℃) and ambient room temperature (25 ℃) for SIM detection in living cells.

Characterization of the Iridium(III) complex dye in living cells

To investigate the cell permeability of the dye in living cells, concentrations of dye ranging from 0.1 to

50 μM were incubated with HeLa cells for 30 min prior to observation under a fluorescence microscope. We observed high phosphorescence accumulation, and even nuclei were stained when cells were exposed to dye at concentrations of 5-50 μM, whereas at concentrations of 0.1, 0.25, and 0.5 μM, phosphorescence intensity was too low to be visible (Supplementary Fig. 5). Taking both into consideration, we determined that the dye at concentrations of 1 and 2.5 μM could be used to image mitochondria well.

Next, we used flow cytometry to quantitatively analyze the cellular uptake of the dye (Supplementary Fig. 6). Results indicated that when the cells were exposed to dye at concentrations greater than 5.0 μM, the cells took up excessive dye, whereas at a concentration less than 2.5 μM, the cellular uptake of the dye gradually decreased in a dose-dependent manner. Thereafter, we evaluated the cytotoxicity of the dye at concentrations of 0.1-50 μM during different durations of incubation using a CCK-8 assay (Supplementary Fig. 7). Under continuous 12-hour co-culture, results revealed no significant differences in cell viability between the control group and the groups treated with the dye at concentrations of less than 10 μM.

Although it is feasible to observe and record dynamic progresses at the cellular level with confocal optical fluorescence microscopy, it is difficult to distinguish subcellular structures at resolutions less than 200 nm due to the Abbe diffraction limit[4, 31, 32]. In response to that problem, after clarifying our dye's excellent cell permeability, high specificity, and low cytotoxicity, we investigated differences between the dye imaging of mitochondria under confocal microscopy and SIM (Supplementary Fig. 8,

Supplementary Movies 1 & 2). To avoid the potential cytotoxicity of high-concentration dyes, we selected 0.5, 1, 2.5, and 5 μM as experimental concentrations. Results revealed that the dye had a low phosphorescence background in confocal microscopy and SIM, as well as that the resolution of the dye at a 1 μM concentration was superior to those at 0.5, 2.5, and 0.5 μM concentrations (Supplementary Fig. 8c, f, i, l). When concentrations exceeded 1 μM, a large amount of the dye was taken up by the cells, which caused strong phosphorescence (Supplementary Fig. 8a-f) that did not meet the requirement for imaging mitochondria at the nanoscale level. By contrast, when the concentration was less than 1 μM, less dye was taken up by the cells, which resulted in weak phosphorescence due to which not even mitochondrial morphology was visible (Supplementary Fig. 8j, i). Therefore, we chose 1 μM as an optimal concentration for further study.

To investigate the photostability and penetration depth of the dye at 1 μM for imaging mitochondria in living cells under SIM, we recorded a single mitochondrion image at every 0.2 μm of depth (Fig. 1e). Results indicated that the dye had uniform tissue permeability at different depths in living cells. The photobleaching properties of the dye directly affected the monitoring of mitochondrial dynamic processes[33, 34]. Next, we performed a long-term continuous laser (165 s) to stimulate cells in order to monitor the photostability of the dye in the same section of the cell (Fig. 1f). We found that the dye had high phosphorescence within 60 s of continuous laser stimulation and could image mitochondria within 135 s without photobleaching. Those properties allowed us to record more dynamic information while monitoring mitochondria in living cells under SIM with the dye.

Whole-cell 3D SIM images of mitochondrial ultrastructures using the Iridium(III) complex dye

Visualizing mitochondrial ultrastructures affords new understandings of the pathology and diagnosis of mitochondria-related diseases[35, 36]. To investigate the capability of obtaining more information about mitochondrial ultrastructures with the dye, we used the dye to image mitochondrial ultrastructures in living cells under 3D SIM. Shown in Fig. 2a, results revealed that after cell incubation with the dye for 30 min, intracellular mitochondria showed spherical, rod-shaped, or filamentous particles approximately 2.0 μm long (Fig. 2c-2) and approximately 0.7 μm wide (Fig. 2c-3), which is consistent with normal mitochondrial volume in HeLa cells (width: 0.5-1.0 μm, length: 1.5-3.0 μm). The lamellar cristae in mitochondrial were also visible using the dye—cristae thickness was approximately 105 nm (Fig. 2b, Supplementary Fig. 9)—and the dye could be evenly distributed on mitochondria (Fig. 2d, Supplementary Movie 3), which suggests that it can be located on the mitochondrial membrane and have high specificity. To further clarify the resolution of the dye for imaging mitochondria, we obtained a full-width at the half-maximum (FWHM) up to 80 nm under SIM (Fig. 2e-f), which is similar to the Atto 647 mitochondrial dye reported by Han et al. (FWHM: 91 nm)[34]. Such results suggest that our dye offers higher resolution and precision for tracking mitochondria under SIM.

Iridium(III) complex dye for tracking mitochondrial dynamics

Mitochondria rank among the most dynamic organelles in cells[34], and understanding their dynamic processes is important for analyzing the causes of many diseases[37]. Therefore, a strategy for visualizing the dynamics of mitochondrial at the nanoscale level has important implications for understanding mitochondria-related diseases. With that goal in mind, we recorded the process of mitochondrial

dynamics using our dye after incubating live cells in it for 30 min (Fig. 3, Supplementary Movie 4). We observed that two mitochondria (Fig. 3d-f, red arrow) maintained a distance of approximately 0.6 μm in Frame 1 (Fig. 3b-1) and gradually approached each other in Frames 1 and 2 (Fig. 3b, e, f). We also observed the separation process of mitochondria, particularly the gradual disintegration from an intact mitochondria (Fig. 3c, g-i, blue arrows), which suggests that our dye can be used to study the dynamic changes of mitochondria.

Application of the Iridium(III) complex dye to track MLC and fusion

The interactions of mitochondria and lysosomes, including fusion involved in mitophagy, are essential for repairing damaged mitochondria. Recently, a direct contact between mitochondria and lysosome was demonstrated in normal living cells[38]. To investigate the crosstalk of mitochondria and lysosomes, we used our dye together with commercial LysoTracker Green to label lysosomes in mammalian cells. We confirmed that mitochondria and lysosomes were close to each other to form MLC, similar to what has been previously reported[38]. We observed that MLC events were normal in wild-type (WT) cells (Fig. 4a-f, Supplementary Fig. 10, Supplementary Movie 5-7), but did not observe fusion. Moreover, we found two types of MLCs (Fig. 4c), point contact with limited overlap (Fig. 4d) and extended contact showing an elongated contact surface (Fig. 4e).

For the application of our dye to image damaged mitochondria related to pathological conditions, we performed another experiment with inducer treatment. We used 10.0 μM carbonyl cyanide m-chlorophenyl hydrazone (CCCP), a common mitochondria damage inducer, to treat cells 12 h prior to

staining with our dye and LysoTracker Green. Compared to untreated cells (Fig. 4g-j, Supplementary Movie 8), we observed a significant increase of large overlaps (yellow spots) of mitochondria and lysosomes corresponding to the fusion after CCCP treatment.

Iridium(III) complex dye to track MLC in Penta knockout HeLa cells

MLCs were observed in both normal and stimulated conditions, while fusion involved in mitophagy was only found after CCCP treatment. Pathologically, PINK1 is recruited to the mitochondrial membrane to phosphorylate Ser65 of ubiquitin ligase and trigger mitophagy. During that process, several receptors (i.e., p62, NDP52, OPTN, NBR1, and TAX1BP1) play an important role[39]. Therefore, it is reasonable to check whether these mitophagy proteins are involved in MLC events other than the recently reported RAB7GTP hydrolysis[38]. To investigate the correlation between MLC and fusion, we performed an experiment with Penta knockout HeLa cells which are deficient of mitophagy. After using 10 μM CCCP to treat cells and staining with our dye and LysoTracker Green, we found MLC events including 2-3 faint yellow spots for point MLC throughout the cells (Fig. 5a-c, Supplementary Movie 9). In addition, we recorded the evolution of an MLC event (Fig. 5d-e, Supplementary Movie 10), in which a mitochondrion and a lysosome underwent approach, contact, and separation. Meanwhile, fusion event involved in mitophagy in Penta KO HeLa cells (Fig. 5a) was disappeared compared to what was found in the WT HeLa cells (Fig. 4g). To that end, we performed a controlled experiment in which Penta KO HeLa cells did not receive CCCP treatment. We detected no significant change of MLC events in Penta KO cells (Fig. 5g, Supplementary Movie 11), which indicates that fusion between mitochondria and lysosomes are independent to MLC. Again, our dye can be used to monitor MLC events in living cells.

Discussion

We discovered that a third-row transition metal complex fluorescent dye based on Iridium(III) can be used to track mitochondrial dynamics under SIM. Using our dye, we obtained a mitochondrial image with approximately 80-nm resolution. We observed mitochondrial cristae and recorded the dynamic approach and separation of mitochondria. Our results provide a novel perspective on using third-row LTMC dyes such as an Iridium(III) complex to image the dynamic process of subcellular structures in living cells under SIM. Given the synthesis of the Iridium(III) complex dye, future work could focus on developing a variety of novel Iridium(III) complex dyes for the specific imaging of lysosomes, mitochondria, cell membranes, nuclei, and other organelles under SIM toward the eventual goal of mapping the organelle interaction network and thereby clarify the network's establishment, maintenance, dynamic changes, and regulatory mechanisms and to reveal its physiological and pathological functions.

Mitochondrial dynamic processes including fusion and fission are closely related to many diseases[40]. With our Iridium(III) complex dye, we have demonstrated the capability of imaging these dynamics with a high special resolution. Moreover, this new Iridium(III) complex dye can also be used to study the functional crosstalk between mitochondria and lysosomes, such as the fusion and MLC. The fusion between mitochondria and lysosomes is an important step of mitophagy for recycling damaged mitochondria[41]. The recently reported formation of MLCs differed from that in mitochondria targeted to lysosomes for destruction[38]. We observed that the fusion of mitochondria and lysosomes can be significantly enhanced upon mitochondrial damage. Five receptors (i.e., p62, NDP52, OPTN, NBR1,

and TAX1BP1) that play essential roles in mitophagy were not involved in the formation of MLCs[38], which suggests MLCs and mitophagy are independent processes.

Methods

Materials

$IrCl_3 \cdot xH_2O$ were purchased from Alfa Aesar, 4,4'-dimethyl-2,2'-bipyridine, diatomite, selenium dioxide 1-phenyl-1,2-propane-dione, 2-aminobenzenethiol and benzene-1,2-diamine were purchased from J&K Scientific. Lyso Tracker Green were purchased from Invitrogen (Invitrogen, Eugene, OR,USA); cell counting kit-8 (CCK-8) was obtained Dojindo Laboratories (Dojindo Laboratories, Kumamoto, Japan); fetal bovine serum (FBS), Dulbecco's modified Eagle's medium (DMEM), and other cell culture reagents were obtained from Gibco BRL (Grand Island, NY, USA).

Synthesis and characterization of Iridium(III) complex dye

The dye was synthesized by using a previously reported protocol [2]. 4'-methyl-[2,2'-bipyridine]-4-carbaldehyde[42] and the auxiliary ligand 2-methyl-3-phenylquinoxaline (mpq)[43] were synthesized according to literature methods. The Iridium(III) dimmer $[Ir(mpq)_2Cl]_2$ was synthesized by using the similar method of $[Ir(ppy)_2Cl]_2$ [44]. The synthetic process of the main ligand and the Iridium(III) complex were according to our previous work.

The main ligand (2-(4'-methyl-[2,2'-bipyridin]-4-yl)benzo[d]thiazole (mbbt)) was synthesized by slowly dropping 2-aminobenzenethiol (196 mg, 1.55 mmol) into the EtOH solution of

4'-methyl-[2,2'-bipyridine]-4-carbaldehyde (297 mg, 1.5 mmol). After stirring overnight in RT, the product was condensed and then recrystallized by using CH_2Cl_2/ethanol to get yellow flaky solid Yield, 80.5%, 367 mg. Anal. Calcd. for $C_{18}H_{13}N_3S$ (%): C, 71.26; H, 4.32; N, 13.85. Found (%): C, 71.03; H, 4.63; N, 13.61.^{1}H NMR (500 MHz, $CDCl_3$) δ 9.27 (s, 1H), 8.60 (d, *J* = 1.0 Hz, 2H), 8.42 (s, 1H), 8.11 (s, 1H), 8.00 (d, *J* = 4.5 Hz, 2H), 7.49 – 7.45 (m, 2H), 7.20 (s, 1H), 2.54 (s, 3H). ES-MS, (CH_3OH): m/z = 304.15 $[M+H]^+$).

The goal Iridium complex were synthesized by mixing mbbt (30.4 mg, 0.1 mmol) and $[Ir(mpq)_2Cl]_2$ (66.3 mg, 0.0525 mmol) in a degassing mixture of chloroform and MeOH(1:1, 40 ml). Then the solution was refluxed overnight in argon atmosphere. After the reaction was stopped, the solvent was removed and further purification was conducted by using alumina column chromatography to get crimson minicrystal. Yield, 51.3%, 49.7 mg. Anal. Calcd. for $C_{48}H_{35}N_7SClIr$ (%): C, 59.46; H, 3.64; N, 10.11. Found (%): C, 59.19; H, 3.91; N, 10.01. ^{1}H NMR (500 MHz, CD_3OD): δ 8.78 (d, *J* = 1.5 Hz, 1H), 8.57 – 8.48 (m, 3H), 8.30 (s, 3H), 8.27 (dd, *J* = 6.0, 1.5 Hz, 1H), 8.23 (d, *J* = 6.0 Hz, 1H), 8.08 (t, *J* = 8.0 Hz, 2H), 7.87 (t, *J* = 8.0 Hz, 2H), 7.59 (s, 1H), 7.57 – 7.51 (m, 4H), 7.42 (t, *J* = 10.0 Hz, 2H), 7.32 – 7.26 (m, 2H), 7.11 (d, *J* = 12.0 Hz, 2H), 6.89 (d, *J* = 8.0 Hz, 2H), 6.72 (dd, *J* = 18.0, 7.5 Hz, 2H), 3.40 (d, *J* = 15.1 Hz, 6H), 2.49 (s, 3H). ^{13}C NMR (125 MHz, CD_3OD) δ164.62, 164.55, 162.30, 156.57, 154.36, 153.18, 152.99, 152.87, 152.81, 152.68, 148.37, 146.82, 144.41, 143.47, 140.06, 139.90, 139.85, 130.62, 130.59, 129.97, 129.88, 129.80, 129.17, 128.66, 127.15, 127.01, 125.14, 125.01, 123.74, 122.98, 122.02, 120.63, 26.14, 26.09, 19.79. ES-MS (CH_3OH): m/z = 933.95 $[M-Cl^-]^+$.

^{1}H and ^{13}C NMR spectra were recorded using a Bruker 500 Nuclear Magnetic Resonance Spectrometer using $CDCl_3$ or CD_3OD as the deuterated solvent. The electronic absorption spectra were recorded using a Perkin-Elmer Lambda 850 UV/Vis spectrometer. The emission spectra were recorded using a Perkin-Elmer LS 55 luminescence spectrometer and FLS 980 luminescence spectrometer. Microanalysis (C, H, and N) was carried out using an Elementar Vario EL elemental analyzer. Electro spray mass spectra were recorded using an LCQ system (Finnigan MAT, USA).

Cell culture

HeLa cells were gifted from Dr. Carolyn M. Price lab (University of Cincinnati). Penta knockout HeLa cells were gifted from Dr. Richard J. Youle lab (National Institutes of Health). Cells were cultured in Dulbecco's modified Eagle medium supplemented with 10% FBS, penicillin (100 units/ml), and streptomycin (100 μg/ml) in a 5% CO_2 humidified incubator at 37 ℃.

Cell viability and cytotoxicity assay

Cells were treated in a 96-well plate at density of 5×10^5 cell/ml. The viability was determined by using a cell counting kit-8 (CCK-8). 10 μl CCK-8 solution was added to each well and the OD value for each well was read at wavelength 450 nm on a microplate reader (Multiskan, Thermo, USA).

Flow cytometry analysis

Cells were seeded on 6-well plate at density of 1×10^5 cell/ml in 1 ml of complete medium for 24 h. After treatment with Iridium(III) complex dye (0.1, 0.25, 0.5, 1, 2.5, 5, 10, 25, and 50 μM) for 30 min, cells were collected by trypsinization and washed 2 times with cool PBS. Cells were resuspended by 500 μl binding buffer while avoiding light prior to detection by flow cytometry.

Live cell labeling

Cells were incubated with 1 μM IR for 30 min in free DMEM, and washed with free DMEM 3 times and observed using a fluorescence microscope (CX41-32RFL; Olympus, Japan), confocal laser scanning microscopy or OMX 3D-SIM super-resolution microscope.

Confocal laser scanning microscopy

The images were obtained using a LSM-710 confocal laser scanning microscope (Carl Zeiss, Inc.) equipped with a 63×/1.49 numerical aperture oil-immersion objective lens and were analyzed with ZEN 2012 (Carl Zeiss, Inc.) and ImageJ software (National Institutes of Health). All fluorescence images were analyzed and the background subtracted with ImageJ software. Pearson's coefficient was quantified using the Colocalisation Analysis plugin for ImageJ.

OMX 3D-SIM super-resolution microscope imaging

Super-resolution images were acquired on OMX 3D-SIM Microscope (Bioptechs, Inc) equipped with a Olympus 100×/1.49 numerical aperture oil-immersion objective lens and solid-state lasers. Images were captured with an electron-multiplying charge coupled device (EMCCD) camera (Photometrics Cascade

II) with a gain value of 3000 at 10 MHz,. The exposure time was set to 50 ms for each raw data capture. Picture was obtained at 512 ×512 using Z-stacks with step size of 0.2 μm. SIM frames were deliberately spaced at 1-s, 2-s, 8-s or 15-s intervals according to the purpose of each experiment. SIM images were analyzed with Nikon Elements and ImageJ software.

Competing financial interests

The authors declare no competing financial interests.

Acknowledgments

This research was supported by 973 Program (Nos. 2015CB856301 and 2015CB856304) from Ministry of Science and Technology of China, the National Science Foundation of China (Nos. 21525105, 21471164, 21778079 and 21701196), China Postdoctoral Science Foundation (20173100041090767), and National Institutes of Health (NIH, R01NS094144 and R01CA211066 to J.G.). The Light Microscopy Imaging Center (LMIC) is supported in part with funds from Indiana University Office of the Vice Provost for Research. The OMX 3D-SIM microscope was provided by NIH grant S10 RR028697. We also thank Dr. Ehmer Birgit at University of Cincinnati for assistance with laser scanning confocal microscope and flow cytometry.

Author contributions

C.J., R.G. and H.C. designed, synthesized and characterized Iridium(III) complex dye. Q.C. and Z.T. collected all OMX 3D-SIM super-resolution microscope data. Q.C and X.S. analyzed and processed the

OMX 3D-SIM data. Q.C., X.S., and C.W. cultured cell and performed confocal laser scanning microscopy. F.L. performed cytotoxicity assay and flow cytometry analysis. J.G., L.J., F.W., H.C., and J.D. conceived the project, designed the experiments, and wrote the manuscript with the help of all authors.

References

1. Arasaki K, Mikami Y, Shames SR, Inoue H, Wakana Y, Tagaya M. Legionella effector Lpg1137 shuts down ER-mitochondria communication through cleavage of syntaxin 17. *Nature Communications* **8**, (2017).

2. Jin CZ, *et al.* Rational design of NIR-emitting iridium(III) complexes for multimodal phosphorescence imaging of mitochondria under two-photon excitation. *Chemical Communications* **53**, 10374-10377 (2017).

3. Picard M, *et al.* Trans-mitochondrial coordination of cristae at regulated membrane junctions. *Nature Communications* **6**, (2015).

4. Huang H, *et al.* Real-time tracking mitochondrial dynamic remodeling with two-photon phosphorescent iridium (III) complexes. *Biomaterials* **83**, 321-331 (2016).

5. Sun L, *et al.* Iridium (III) anthraquinone complexes as two‐photon phosphorescence probes for mitochondria imaging and tracking under hypoxia. *Chemistry-A European Journal* **22**, 8955-8965 (2016).

6. Watanabe S, *et al.* Protein localization in electron micrographs using fluorescence nanoscopy. *Nature Methods* **8**, 80-U117 (2011).

7. Heller I, *et al.* STED nanoscopy combined with optical tweezers reveals protein dynamics on densely covered DNA. *Nature Methods* **10**, 910-U132 (2013).

8. Li DY, Qin W, Xu B, Qian J, Tang BZ. AIE Nanoparticles with High Stimulated Emission Depletion Efficiency and Photobleaching Resistance for Long-Term Super-Resolution. *Adv Mater* **29**, (2017).

9. Li D, *et al.* Extended-resolution structured illumination imaging of endocytic and cytoskeletal dynamics. *Science* **349**, (2015).

10. Huang X, *et al.* Fast, long-term, super-resolution imaging with Hessian structured illumination microscopy. *Nat Biotechnol*, (2018).

11. Shao L, Kner P, Rego EH, Gustafsson MGL. Super-resolution 3D microscopy of live whole cells using structured illumination. *Nature Methods* **8**, 1044-+ (2011).

12. Wombacher R, *et al.* Live-cell super-resolution imaging with trimethoprim conjugates. *Nature Methods* **7**, 717-719 (2010).

13. Huang B, Jones SA, Brandenburg B, Zhuang XW. Whole-cell 3D STORM reveals interactions between cellular structures with nanometer-scale resolution. *Nature Methods* **5**, 1047-1052 (2008).

14. Jones SA, Shim SH, He J, Zhuang XW. Fast, three-dimensional super-resolution imaging of live cells. *Nature Methods* **8**, 499-U496 (2011).

15. Ha T, Tinnefeld P. Photophysics of Fluorescent Probes for Single-Molecule Biophysics and Super-Resolution Imaging. *Annu Rev Phys Chem* **63**, 595-617 (2012).

16. Huang B, Bates M, Zhuang XW. Super-Resolution Fluorescence Microscopy. *Annu Rev Biochem* **78**, 993-1016 (2009).

17. Subach FV, Patterson GH, Manley S, Gillette JM, Lippincott-Schwartz J, Verkhusha VV. Photoactivatable mCherry for high-resolution two-color fluorescence microscopy. *Nature Methods* **6**, 153-159 (2009).

18. Day RN, Davidson MW. The fluorescent protein palette: tools for cellular imaging. *Chemical Society Reviews* **38**, 2887-2921 (2009).

19. Grimm JB, *et al.* A general method to improve fluorophores for live-cell and single-molecule microscopy. *Nature methods* **12**, 244 (2015).

20. Kim HM, Cho BR. Small-molecule two-photon probes for bioimaging applications. *Chemical reviews* **115**, 5014-5055 (2015).

21. Wolfbeis OS. An overview of nanoparticles commonly used in fluorescent bioimaging. *Chemical Society Reviews* **44**, 4743-4768 (2015).

22. Chen Y, Rees TW, Ji L, Chao H. Mitochondrial dynamics tracking with iridium (III) complexes. *Current opinion in chemical biology* **43**, 51-57 (2018).

23. Saeed HK, *et al.* Homo- and Heteroleptic Phototoxic Dinuclear Metallo-Intercalators Based on Ru-II(dppn) Intercalating Moieties: Synthesis, Optical, and Biological Studies. *Angew Chem Int Edit* **56**, 12628-12633 (2017).

24. Fernandez-Moreira V, Thorp-Greenwood FL, Coogan MP. Application of d(6) transition metal complexes in fluorescence cell imaging. *Chemical Communications* **46**, 186-202 (2010).

25. Nam SH, *et al.* Long-Term Real-Time Tracking of Lanthanide Ion Doped Upconverting Nanoparticles in Living Cells. *Angew Chem Int Edit* **50**, 6093-6097 (2011).

26. Zhang PY, *et al.* A NIR phosphorescent osmium(II) complex as a lysosome tracking reagent and photodynamic therapeutic agent. *Chemical Communications* **53**, 12341-12344 (2017).

27. Tang J, *et al.* A photoactivatable Znsalen complex for super-resolution imaging of mitochondria in living cells. *Chemical Communications* **52**, 11583-11586 (2016).

28. Sreedharan S, *et al.* Multimodal Super-resolution Optical Microscopy Using a Transition-Metal-Based Probe Provides Unprecedented Capabilities for Imaging Both Nuclear Chromatin and Mitochondria. *Journal of the American Chemical Society* **139**, 15907-15913 (2017).

29. You Y. Phosphorescence bioimaging using cyclometalated Ir (III) complexes. *Current opinion in chemical biology* **17**, 699-707 (2013).

30. Chen Y, Zhu C, Cen J, Bai Y, He W, Guo Z. Ratiometric detection of pH fluctuation in mitochondria with a new fluorescein/cyanine hybrid sensor. *Chemical science* **6**, 3187-3194 (2015).

31. Schermelleh L, *et al.* Subdiffraction multicolor imaging of the nuclear periphery with 3D structured illumination microscopy. *Science* **320**, 1332-1336 (2008).

32. Huang B, Babcock H, Zhuang XW. Breaking the Diffraction Barrier: Super-Resolution Imaging of Cells. *Cell* **143**, 1047-1058 (2010).

33. Li X, Jiang M, Lam JW, Tang BZ, Qu JY. Mitochondrial Imaging with Combined Fluorescence and Stimulated Raman Scattering Microscopy Using a Probe of the Aggregation-Induced Emission Characteristic. *Journal of the American Chemical Society* **139**, 17022-17030 (2017).

34. Han Y, Li M, Qiu F, Zhang M, Zhang Y-H. Cell-permeable organic fluorescent probes for live-cell long-term super-resolution imaging reveal lysosome-mitochondrion interactions. *Nature communications* **8**, 1307 (2017).

35. Kopek BG, Shtengel G, Xu CS, Clayton DA, Hess HF. Correlative 3D superresolution fluorescence and electron microscopy reveal the relationship of mitochondrial nucleoids to membranes. *Proceedings of the National Academy of Sciences* **109**, 6136-6141 (2012).

36. Manji H, *et al.* Impaired mitochondrial function in psychiatric disorders. *Nature Reviews Neuroscience* **13**, 293 (2012).

37. Buck MD, *et al.* Mitochondrial dynamics controls T cell fate through metabolic programming. *Cell* **166**, 63-76 (2016).

38. Wong YC, Ysselstein D, Krainc D. Mitochondria–lysosome contacts regulate mitochondrial fission via RAB7 GTP hydrolysis. *Nature* **554**, 382 (2018).

39. Lazarou M, *et al.* The ubiquitin kinase PINK1 recruits autophagy receptors to induce mitophagy. *Nature* **524**, 309 (2015).

40. Chan DC. Mitochondrial fusion and fission in mammals. *Annu Rev Cell Dev Biol* **22**, 79-99 (2006).

41. Youle RJ, Narendra DP. Mechanisms of mitophagy. *Nature reviews Molecular cell biology* **12**, 9 (2011).

42. Peek BM, Ross GT, Edwards SW, Meyer GJ, Meyer TJ, Erickson BW. Synthesis of redox derivatives of lysine and related peptides containing phenothiazine or tris (2, 2′‐bipyridine) ruthenium (II). *Chemical Biology & Drug Design* **38**, 114-123 (1991).

43. Zhang Z, Du H. A Highly cis‐Selective and Enantioselective Metal‐Free Hydrogenation of 2, 3‐Disubstituted Quinoxalines. *Angewandte Chemie International Edition* **54**, 623-626 (2015).

44. Nonoyama M. Benzo [h] quinolin-10-yl-N Iridium (III) Complexes. *Bulletin of the Chemical Society of Japan* **47**, 767-768 (1974).

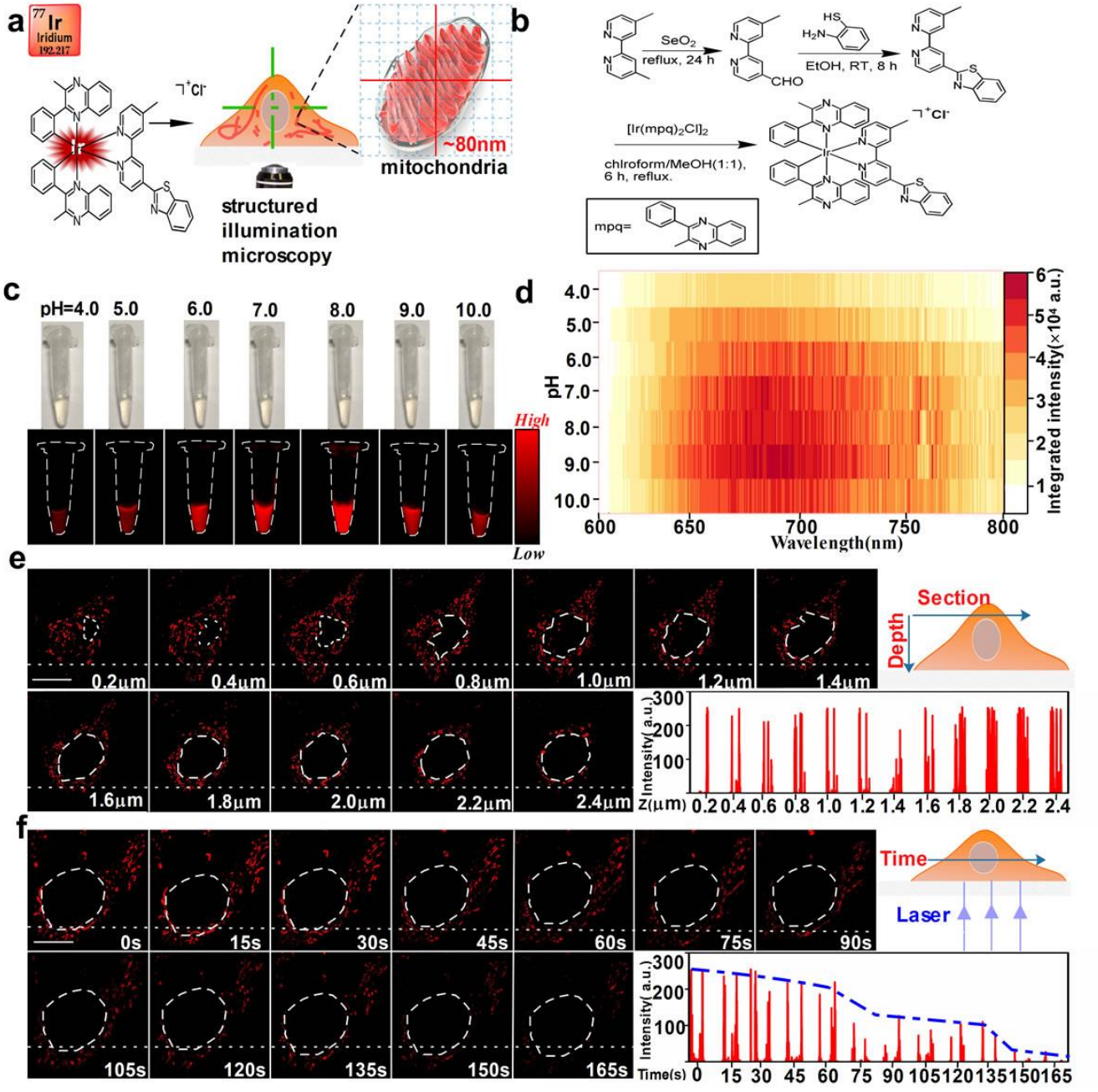

Figure 1 Synthesis and optical characterization of the Iridium(III) complex dye. (a) Schematic representation of the Iridium(III) complex dye while imaging mitochondria under SIM. **(b)** Synthesis route of the Iridium(III) complex dye. **(c)** Fluorescence image of the Iridium(III) complex dye in phosphate-buffered saline at different pH levels. **(d)** Photoluminescence mapping of the Iridium(III) complex dye. **(e)** Mitochondrial images at different depths using the Iridium(III) complex dye. White

488 dotted lines show fluorescence intensity of a single mitochondrion image at every depth of 0.2 μm. **(f)**
489 Photobleaching properties of the Iridium(III) complex dye under laser stimulation for 165 s continuously
490 recorded in living cells. SIM frames were deliberately spaced at 15-s intervals. Scale bars: **e** 5 μm, **f** 5
491 μm.
492

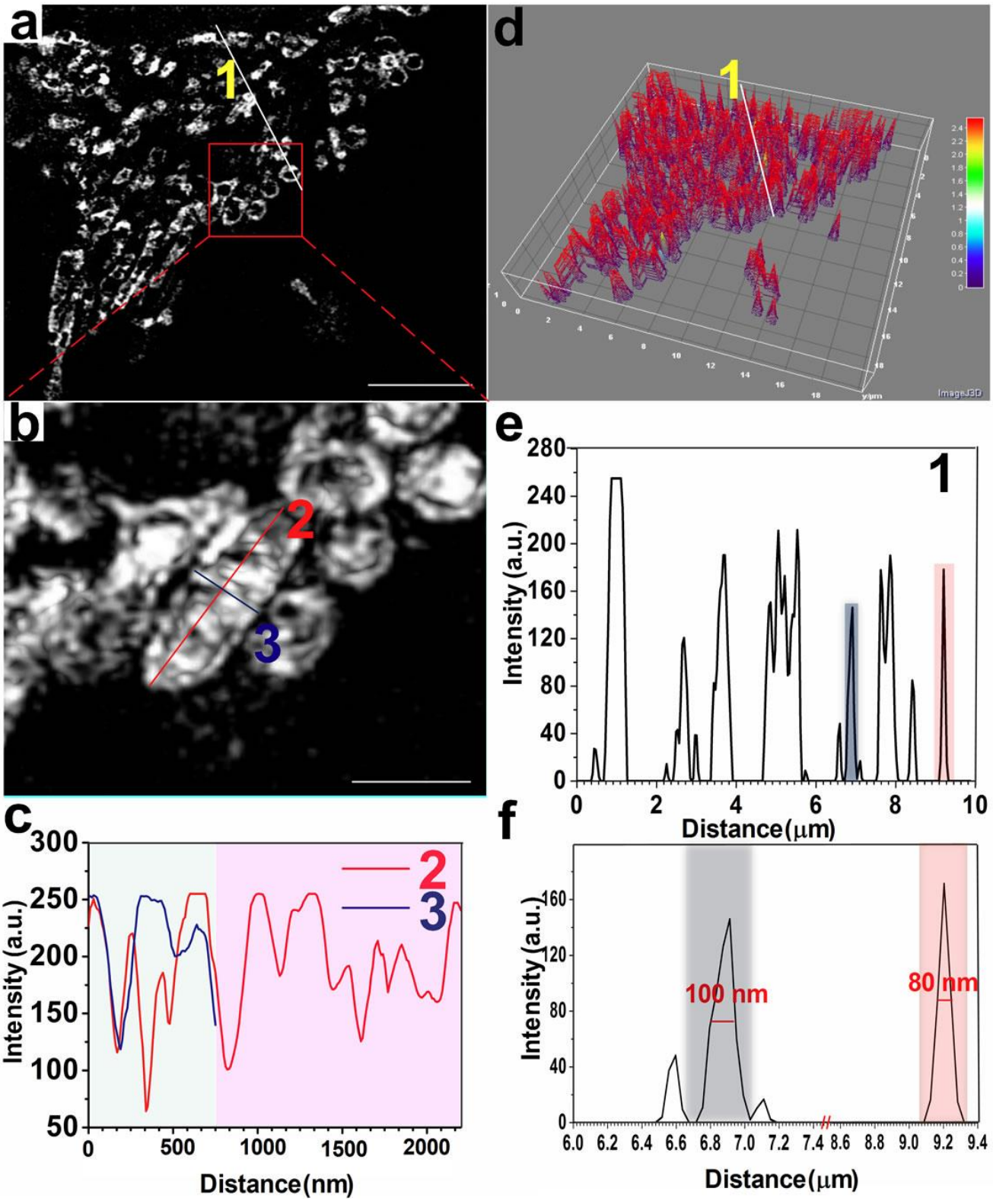

493

494 **Figure 2 Iridium(III) complex dye images of mitochondrial ultrastructure. (a)** Iridium(III) complex

dye images of mitochondria in 1 μM concentration under 3D SIM. White solid line **1** shows fluorescence intensity, and red rectangle shows partial amplification. **(b)** Single mitochondrial local enlargement of **a**. Red solid line **2** shows the length of a single mitochondrion, and blue solid line **3** shows its width. **(c)** Individual mitochondria fluorescence intensity with length as red solid line **2** and width as blue solid line **3. (d)** Iridium (III) complex dye 3D map distributed in mitochondria under SIM. **(e)** Fluorescent intensity distribution of white solid line **1**. **(f)** Local magnification of **e**, with resolution of Iridium(III) complex dye image of mitochondria up to 80 nm. Scale bars: **a** 5 μm, **b** 1 μm.

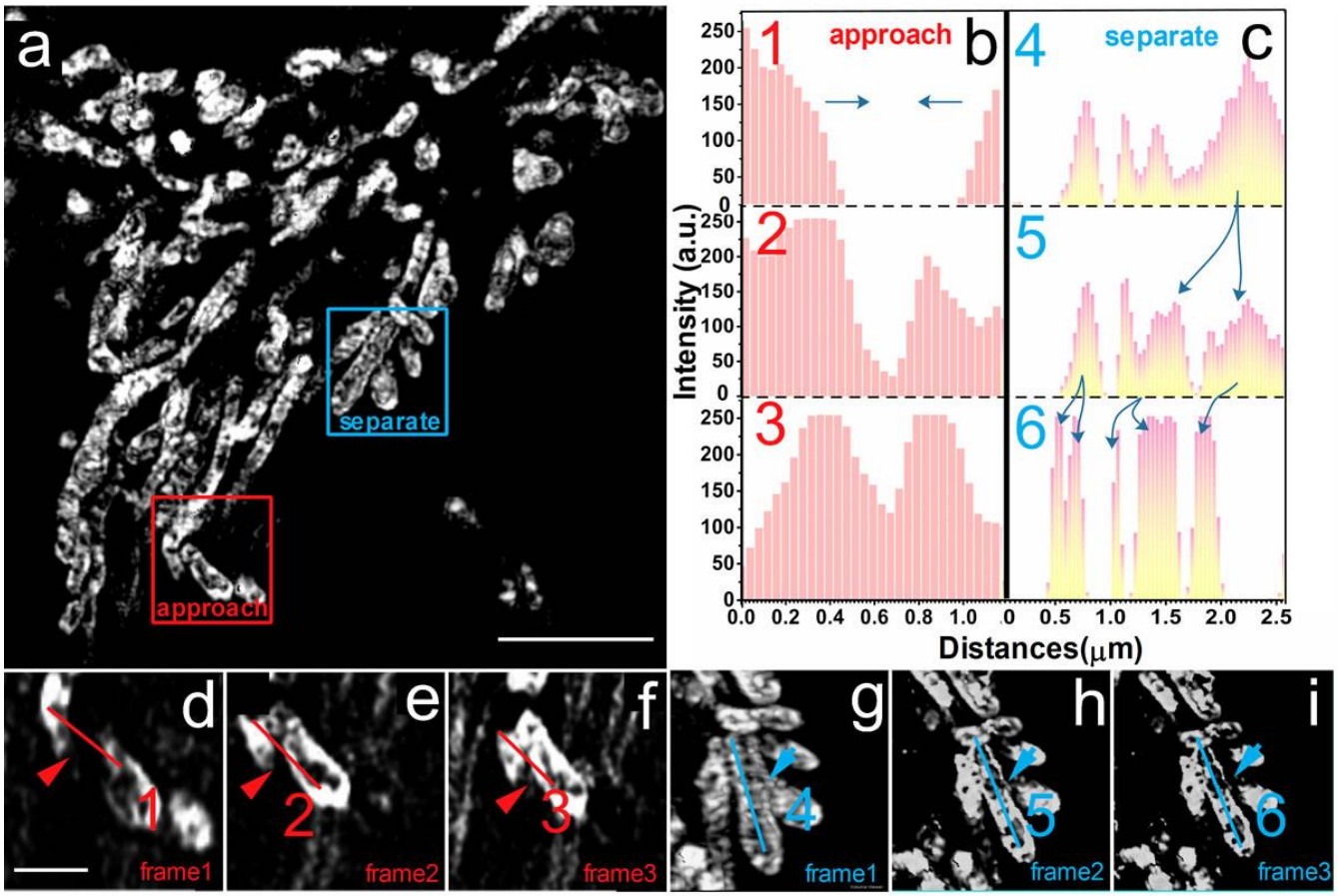

Figure 3 Iridium(III) complex dye tracking of mitochondrial dynamics under SIM. (a) Iridium(III) complex dye images of mitochondria under SIM. Red rectangles indicate dynamic processes of approach, and blue rectangles indicate dynamic processes of separation. **(b)** Trend of fluorescence intensity in the dynamic process of approach. **(c)** Trend of fluorescence intensity in the dynamic process of separation. **(d-f)** Frames 1-3 of the dynamic approach process in the red rectangle of **a**. **(g-i)** Frames 4-6 of the dynamic separation process in the blue rectangle of **a**. The time interval between each frame is approximately 2 s. Both red and blue solid lines show fluorescence intensity. Scale bars: **a** 5 μm, **d** 1 μm.

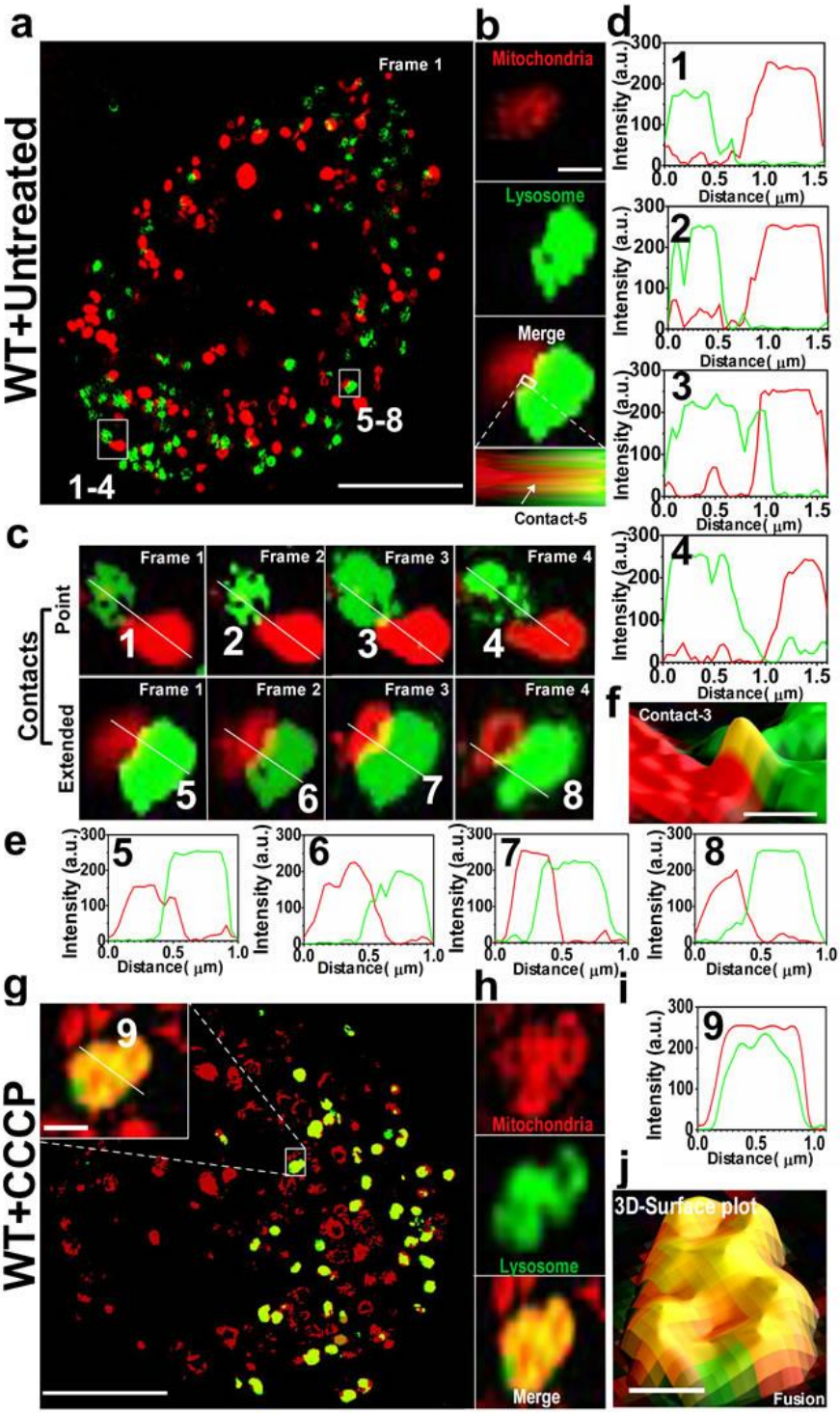

Figure 4 Iridium(III) complex dye tracking of mitochondria–lysosome contact (MLC) and fusion events in living cells. (a) MLC events in WT cells. White rectangles represent two types of MLCs, point (1-4) and extended (5-8) contacts. (**b**) A representative MLC event. White rectangle represents the

516 amplification. (**c**) Point and extended MLCs in (**a**). White solid lines indicate the fluorescence intensity
517 shown in (**d**) and (**e**). (**f**) Partial enlargement of **d**-3. (**g**) fusion events in WT cells after treatment CCCP.
518 White rectangle shows the representative fusion event, and the white solid line shows fluorescence
519 intensity. (**h**) A representative fusion event detected by using the Iridium(III) complex dye (red,
520 mitochondria) and LysoTracker Green (green, lysosome). (**i**) Fluorescence intensity of the solid line of
521 **g**-9 inset. (**j**) 3D SIM surface plot of merged image in **h**. Scale bars: **a** 5.0 μm, **b** 0.5 μm, **e** 0.2 μm, **g** 5.0
522 μm, **g** 0.5 μm, **j** 0.5 μm.
523

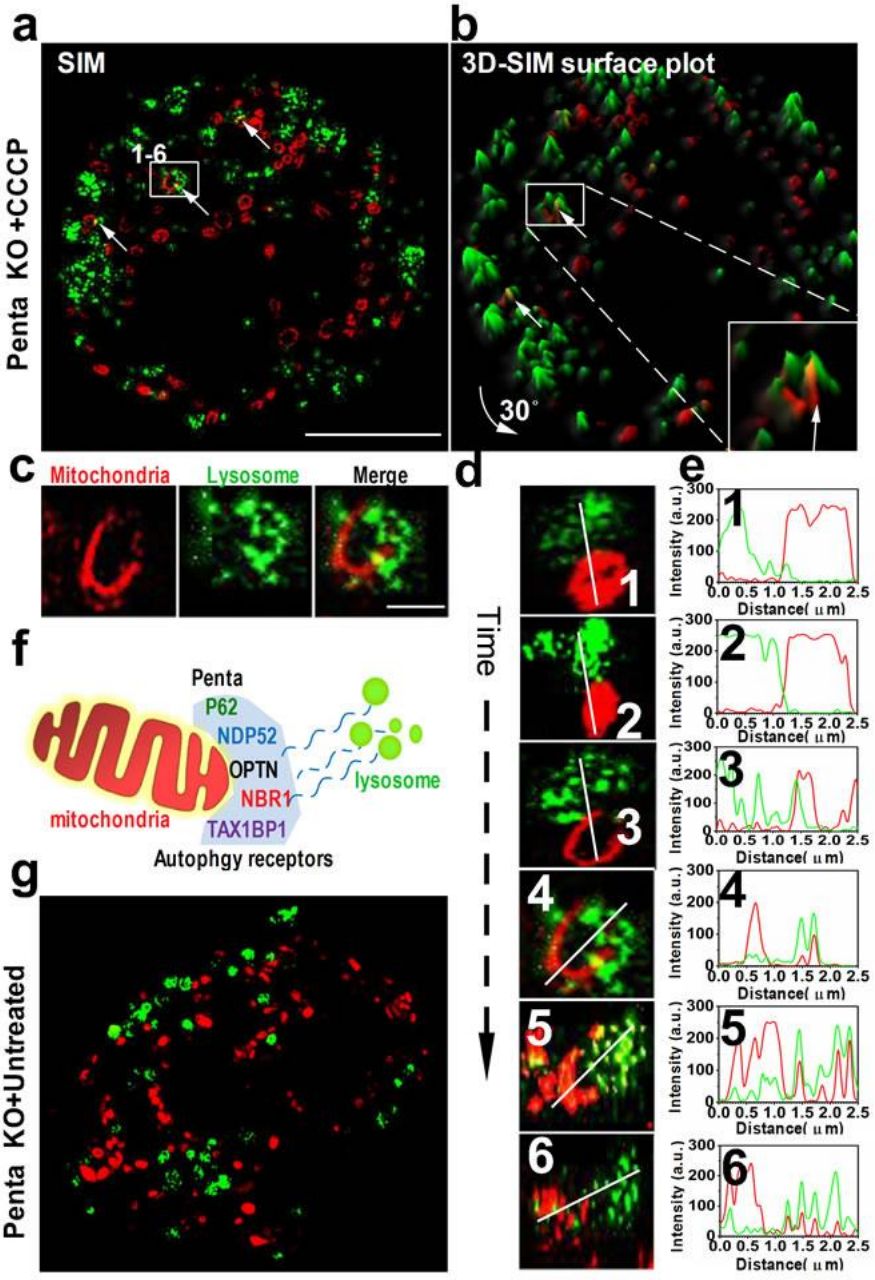

Figure 5 Iridium(III) complex dye for tracking MLC in Penta knockout HeLa cells. (**a**) MLC events in Penta KO cells treated with 10 μM CCCP for 12 h. White rectangle represents the MLC shown in (**d**). **(b)** 3D SIM surface plot of (**a**) after 30-degree rotation. White arrows indicate the MLC events. **(c)** A representative MLC event. (**d**) Time evolution of one MLC in living cell. White solid lines indicate fluorescence intensity shown in (**e**). Scale bars: **a** 5.0 μm, **b** 1.0 μm.